Random-walk approach to mapping nodal regions of *N*-body wave functions: Ground-state Hartree–Fock wave functions for Li–C

William A. Glauser, Willard R. Brown, and William A. Lester, Jr.
Department of Chemistry, University of California, Berkeley, California 94720 and Chemical Sciences Division, Lawrence Berkeley Laboratory, 1 Cyclotron Road, Berkeley, California 94720

D. Bressanini
Dipartimento di Chimica Fisica ed Elettrochimica, Universita' di Milano, Via Golgi 19, Milano, Italy 20133

Brian L. Hammond
Fujitsu America Inc., 3055 Orchard Drive, San Jose, California 95134

M. L. Koszykowski
Combustion Research Facility, Sandia National Laboratories, Livermore, California 94551

(Received 11 June 1992; accepted 10 September 1992)

Despite the widespread acceptance of the relevance of the nodes of one-body electronic wave functions (atomic or molecular orbitals) in determining chemical properties, relatively little is known about the corresponding nodes of many-body wave functions. As an alternative to mapping the nodal surfaces present in the ground states of many-electron systems, we have focused instead on the structural domains implied by these surfaces. In the spirit of Monte Carlo techniques, the nodal hypervolumes of a series of atomic N-body Hartree–Fock level electronic wave functions have been mapped using a random-walk simulation in $3N$ dimensional configuration space. The basic structural elements of the domain of atomic or molecular wave functions are identified as nodal regions (continuous volumes of the same sign) and permutational cells (identical building blocks). Our algorithm determines both the relationships among nodal regions or cells (topology) as well as the geometric properties within each structural domain. Our results indicate that ground-state Hartree–Fock wave functions generally consist of four equivalent nodal regions (two positive and two negative), each constructed from one or more permutational cells. We have developed an operational method to distinguish otherwise identical permutational cells. The limitations and most probable sources of error associated with this numerical method are discussed as are directions for future research.

I. INTRODUCTION

One of the most fundamental attributes of wave functions is nodal structure. Nodes serve to divide the domain of the wave function into regions of positive and negative sign. For a given atomic or molecular system, there is a one-to-one correspondence between the nodal structure and the electronic state. Because mental imagery is limited to three dimensions, one-body wave functions for systems such as the particle-in-a-box, harmonic oscillator, or hydrogenlike atoms are often used to introduce the subject. Since wave functions for N-body systems have a $3N$-dimensional domain (e.g., 6 for the electronic wave function of helium), intuition will not generally serve as a useful guide in trying to visualize the nodes of a many-body wave function. Anderson[1,2] and Barnett *et al.*[3] characterized the nodes of very simple many-body systems (He and H_3, respectively) by constructing three-dimensional (3D) cross sections through the full $3N$-dimensional space by fixing the positions of all but one particle. Unfortunately, the problem of building up $3N$ space from 3D slices scales exponentially with N and cannot be readily extended to larger systems. In a recent article, Ceperley provided a careful analysis and summary of what little is known about the nodes of many-body fermion wave functions and introduced some of the general properties that the nodes of the wave function for an electron gas are expected to possess.[4] Our goal is to broaden the scope of this seminal work to chemical systems (e.g., bound atomic systems) and to deduce specific geometric properties of wave functions by computational studies.

Ab initio wave functions such as Hartree–Fock (HF), multiconfigurational HF, and configuration interaction (CI) are variational. Because HF energies are not affected by first-order changes in the wave function, they are relatively insensitive to small perturbations in the placement of nodal surfaces. Furthermore, because contributions to the variational integral are proportional to the square of the wave function, such calculations are necessarily biased toward providing better descriptions of regions where $|\Psi|$ has large amplitude. This property has made possible tremendous progress in the *ab initio* calculation of energies, but properties that depend sensitively upon a more global description of Ψ (e.g., multipole moments) have not fared as well. Indeed, it is usually considered a virtue that variational methods yield better energies than wave functions. When very accurate energies are sought using basis-set methods, such as configuration interaction (CI), however, this advantage is diminished due to difficulty in describing

 0021-9606/92/249200-16$06.00

the electron–electron cusp behavior and the curvature of the wave function near the nodes.

Nodal considerations are of immediate practical importance when quantum Monte Carlo (QMC) is used to solve the Schrödinger equation.[5] In QMC, the exact ground state of the time-independent Schrödinger equation, $\Phi_0(\mathbf{R})$, can be projected out from any initial distribution $\Psi(\mathbf{R},0)$ not orthogonal to $\Phi_0(\mathbf{R})$ using the time-evolution operator written in *imaginary* time:

$$\exp(-t\hat{H})\,|\Psi(\mathbf{R},0)\rangle \overset{\lim t\to\infty}{=} |\Psi(\mathbf{R},\infty)\rangle = \Phi_0(\mathbf{R}). \quad (1)$$

The time-dependent Schrödinger equation transformed to imaginary time may be viewed as a classical diffusion equation, along with a birth/death process that mimics a reaction exhibiting first-order kinetics:

$$-\frac{\partial\Psi(\mathbf{R},t)}{\partial t} = (-D\nabla^2 + V)\Psi(\mathbf{R},t) \overset{\lim t\to\infty}{=} 0. \quad (2)$$

This interpretation requires the wave function, rather than its square, to be considered a probability density. While this presents no difficulties in the symmetric (boson) ground state, excited-state wave functions (including the fermion ground-state wave function) change sign as nodes are crossed and the classical analogy breaks down.

In some cases, QMC simulations employ the technique of importance sampling,[6] whereby a trial wave function $\Psi_T(\mathbf{R})$ is used to bias the random walk so as to sample from a different probability distribution $f(\mathbf{R},t)$, where

$$f(\mathbf{R},t) \overset{\lim t\to\infty}{=} \Psi_T(\mathbf{R})\Psi(\mathbf{R},\infty) = \Psi_T(\mathbf{R})\Phi_0(\mathbf{R}). \quad (3)$$

Here $\Phi_0(\mathbf{R})$ refers to the boson ground state. For the diffusion analogy to hold in this case, it is necessary that $f(\mathbf{R},t)$ rather than $\Psi(\mathbf{R},t)$ remain positive definite. One way to project out the fermion ground state (or any other excited state) is to employ the fixed-node approximation,[2] in which the nodes of $\Psi_T(\mathbf{R})$ are imposed as a boundary condition upon the evolving solution $\Psi(\mathbf{R},t)$. This boundary condition ensures that $f(\mathbf{R},t)$ is positive definite since $\Psi_T(\mathbf{R})$ and $\Psi(\mathbf{R},t)$ will have the same sign for all $\mathbf{R}$. If the nodes of Ψ_T coincide with those of the exact wave function Φ_0, the fixed-node QMC energy will be exactly E_0 (i.e., there would be no inaccuracy). The extent to which Ψ_T differs from Φ_0 elsewhere determines the statistical variance of E_0. For this reason, one may wish to optimize the nodal surfaces without significantly altering Ψ_T elsewhere.[7]

In short, the most straightforward way to assess the quality of the nodal surfaces of Ψ_T is to compare the fixed-node QMC energy (E_{FN}) with E_0. This is usually an expensive undertaking since the statistical error associated with E_{FN} must be reduced to a very small value to enable a meaningful assessment of differences between E_{FN} and E_0. Furthermore, with the exception of very small systems, E_0 is not accurately known. If the nodes of Ψ_T are sufficiently close to those of the exact wave function Φ_0, perturbative methods such as the released node method[8] can be applied to obtain the exact result. However, these methods are extremely costly and inherently unstable. Variational calculations only guarantee lower energies as more flexibility is introduced by successively increasing the size of the basis set or number of interacting configurations in the trial wave function. However, the quality of the nodes is not guaranteed to improve monotonically in this fashion. Although random statistical error can be made arbitrarily small by large-scale sampling, the systematic error caused by the fixed-node approximation will remain. It is therefore a challenge to seek other properties that are indicative of the overall quality of the nodal surfaces. Rather than look at other indirect indicators, such as multipole moments or polarizabilities, we have instead chosen to study the properties of the nodal surfaces directly. We note here that not all QMC methods impose the fixed-node approximation. Recently methods have been proposed to impose antisymmetry directly upon the QMC solution to obtain the exact energy without the need for exact nodes.[9a–9c] Although these methods hold much promise for transcending the fixed-node approximation in the ground state, they are presently limited in scope.

Despite the considerable mathematical literature devoted to the formal properties of the nodes of L^2 solutions to the Schrödinger equation,[10] no *analytical* representations are available for these nodal surfaces. An exhaustive *numerical* mapping of the nodal hypersurfaces is a prohibitively expensive undertaking for even the smallest systems, and would yield a bewildering array of numbers lacking in direct significance. Here we instead examine the topological and geometric properties of the nodal hypervolumes enclosed by these surfaces. Furthermore, our approach enables us to study structural elements in the domain of the wave function that are not necessarily delimited by nodal surfaces. Our long-range goal is to understand the relationship between antisymmetry nodes and excitation (orthogonality) nodes that coexist in fermion excited states (e.g., excited electronic states of atoms or molecules). Therefore, we begin by examining the properties of antisymmetry nodes alone, which are the only nodes present in fermion ground states. Indeed, the manifold of fermion states and boson states differs only by the presence of antisymmetry node(s) in the fermion states.

In this paper, we present a simple method to explore nodal topology and subsequently apply it to ground-state Hartree–Fock wave functions of some first-row atoms. The next section contains background information on the nodes of N-body wave functions. In Sec. III, we introduce an extension to Ceperley's methodology of mapping nodal regions with a random walk. In Sec. IV, we report the results of the application of our approach to HF wave functions of Li–C.

II. GENERAL NODAL PROPERTIES

The full nodal hypersurfaces of a continuous spatial function of $3N$ coordinates are of dimension $3N-1$, dividing $3N$ dimensional configuration space of the N electrons into nodal regions of opposite sign. Each of the $3N$ coordinates corresponds to a degree of freedom (e.g., x, y, z) of a particular electron. Klein and Pickett[11] have pointed out that symmetry requirements only determine a $3N-3$ dimensional subsurface or hyperpoint where two electrons

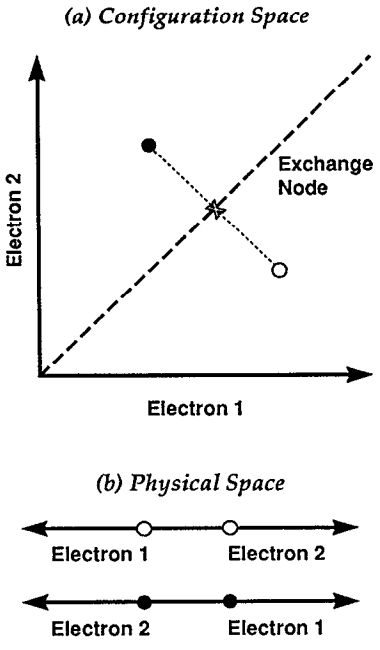

FIG. 1. Example of a random walker in (a) two-dimensional configuration space representing (b) two electrons in one-dimensional physical space. Relection through the antisymmetry (exchange) node depicted in (a) corresponds to a permutation of the two electrons depicted in (b).

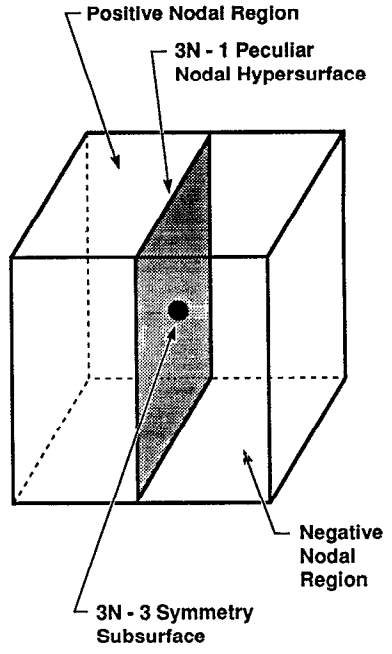

FIG. 2. Representation of symmetry vs peculiar nodal hypersurfaces.

are coincident. In one dimension, two electrons can exchange only by passing through each other (see Fig. 1), but in higher dimensions this is not necessary. Since a permutation of the coordinates of two electrons must result in the wave function changing sign, every exchange pathway will entail a nodal crossing. These additional nodal points (beyond those lying within the hyperpoint) describe the remainder of the $3N-1$ hypersurface. According to Caffarel and Claverie,[12a,12b] the full nodal hypersurface thus consists of the *symmetry* subsurface ($3N-3$ dimensional), which is independent of the wave function and known exactly, and the *peculiar* nodal hypersurface ($3N-1$ dimensional), which will in general not be given by any symmetries (except for very simple systems such as the $1\,^3S$ state of He). This is shown in Fig. 2. The additional information required for the complete specification of the nodal hypersurfaces is only available *a posteriori* from the solution of the Schrödinger equation and is defined by both the form of the potential and the antisymmetry constraint.

In order to discuss symmetry properties of wave functions it is useful to appeal to the full molecular Hamiltonian group $\mathbf{G}_{\text{full}}$,[13]

$$\mathbf{G}_{\text{full}}=\mathbf{G}_T\otimes\mathbf{K}(\text{spatial})\otimes\mathbf{S}_n^{(e)}\otimes\mathbf{G}^{(\text{CNP})}\otimes E \tag{4}$$

which is given as the direct product of the translational ($\mathbf{G}_T$), rotational [$\mathbf{K}$ (spatial)], electron permutation ($\mathbf{S}_n^{(e)}$), nuclear permutation ($\mathbf{G}^{(\text{CNP})}$), and inversion groups (E). The elements of these groups commute with the molecular Hamiltonian and provide true symmetry labels for the corresponding eigenfunctions. The symmetry elements of the molecular point group do not commute with the complete molecular Hamiltonian but only with the vibronic Hamiltonian. For fermions, we are particularly interested in the antisymmetric irreducible representation of the electron permutation group $\mathbf{S}_n^{(e)}$ which has character $(+1)$ under all even permutations and character (-1) under all odd permutations.

The permutation operator $\hat{P}$ permutes both spatial ($\mathbf{R}$) *and* spin (Σ) coordinates of a given pair of electrons,

$$\hat{P}\Psi(\mathbf{R},\Sigma)=(-1)^P\Psi(\mathbf{R},\Sigma), \tag{5}$$

and yields $N!$ permutations, where N is the number of electrons. A Slater determinant is a function of $3N$ spatial coordinates and N spin coordinates and does not possess spatial nodes per se. In this $4N$ dimensional domain, the $4N-1$ dimensional nodal hypersurfaces defy simple interpretation. By fixing the spin coordinates, however, we may examine the spatial nodes directly. For any given total electronic spin, the particular spin configuration adopted is not important here since different configurations merely correspond to a relabeling of the electrons. In QMC, this prescription is used to sample the energy and any other spin-independent quantity. In this paper, we shall use the familiar Coulombic Hamiltonian throughout; no magnetic interactions are available to flip spins. In this case, α-spin electrons no longer permute with β-spin electrons and the full Slater determinant factors into α-spin and β-spin determinants thus reducing the number of allowed permutations from $(N_\alpha+N_\beta)!$ to $N_\alpha!N_\beta!$.

We define a nodal region as a set of all points in a region of $3N$ space that can be interconnected without crossing a node (this is a nodal *cell* by Ceperley's definition[4]). Each nodal region is constructed from one or more *permutational cells* which, in a sense, are the fundamental building blocks for the $3N$ space of fermion wave functions (see Fig. 3). Ceperley has proven that a tilting property exists for ground-state fermion systems: there is only one

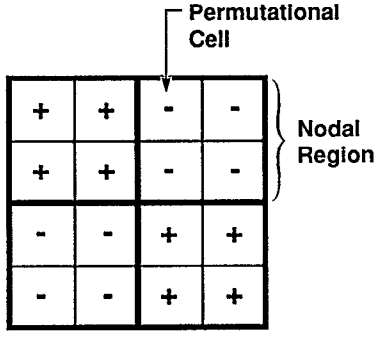

FIG. 3. Relationship between nodal regions and permutational cells.

unique permutational cell insofar as all other cells are just mirror-image permutational reflections of any given cell. Note that this statement provides an *implicit* definition of permutational cells. For fully polarized free-particle systems (i.e., completely spin-aligned systems), there is only one positive and one negative nodal region (i.e., all cells within a positive region are interconnected, and all cells within a negative region are interconnected). We wish to determine whether this result also holds for bound-state Hartree–Fock wave functions. No *a priori* prescription exists for partitioning nodal regions into permutational cells. Since neighboring cells of the same sign may cohabit a contiguous volume, there may not exist explicit boundaries between them. Permutational cells can only be *explicitly* defined by construction; selecting an arbitrary point together with all related permutational images adds one point to each permutational cell.

It is possible to study the nodal properties of ground states for systems of arbitrary size only because of the permutational symmetry expected. The number of permutational cells increases factorially with the number of electrons. In the case of a closed-shell system with 20 electrons, for example, it would require insuperable computation time to map the 10!10! permutational cells that are present in the ground state. By restricting our attention to the properties of a *single* permutational cell, which also describes the properties of every other cell, it becomes possible to subject systems possessing any number of electrons to this method of inquiry. Insofar as antisymmetry provides only $3N-3$ hyperpoints, the choice of M equivalent permutational cells is not unique; different wave functions will, in general, yield a *different* set of equivalent permutational cells. In HF-based treatments, the potential appearing in the Fock operator is specified by the wave function itself. Because the $3N-1$ *peculiar* hypersurface is specified by the potential, it follows that it is also specified by the wave function.

Antisymmetry is inherently a many-body phenomenon. One-body wave functions such as atomic orbitals possess only excitation nodes. Ceperley has pointed out that the nodes of an N-body wave function have little to do with those of the corresponding orbitals.[4] This can be readily illustrated for the first triplet state of He, where we may write a general self-consistent-field (SCF) wave function in the form

$$^3\Psi(1,2)=\psi_1(1)\psi_2(2)-\psi_1(2)\psi_2(1), \tag{6}$$

where $\psi_i(j)$ is an atomic spin orbital. If one of the electrons is on a node of one of the spin orbitals, the wave function is not required to vanish since in an antisymmetrized wave function another term in the determinantal expansion will exist where that electron is in a different spin orbital. $\Psi(1,2)$ in Eq. (6) will be required to vanish only when the two terms are equal. If the N-body wave function is expressed only as a simple product of one-particle states (i.e., no antisymmetrization or symmetrization), the nodes of $\Psi(1,2)$ would correspond to and be exclusively determined by those of $\psi_1(1)$ and $\psi_2(2)$ individually. We note that N-body antisymmetry nodes would be present even if all the occupied orbitals were nodeless (e.g., spin orbitals that result from a relativistic treatment), except for the ground states of two-electron systems where spatial antisymmetry is necessarily absent.

In the case of ^3S states of He, the wave function can be expressed exactly as a function of the electron-nuclear distances r_1 and r_2, and the interelectronic distance r_{12}. Since the wave function must be antisymmetric with respect to exchange of electrons 1 and 2, and $r_{12}=r_{21}$, then $\Psi(r_1,r_2,r_{12})=-\Psi(r_2,r_1,r_{21})$. If $r_1=r_2$, then $\Psi=0$. This constitutes one of the few cases where symmetry considerations provide the $3N-1$ dimensional *peculiar* hypersurface *a priori*. In contrast, the nodal surfaces of the $2s$ atomic orbitals are given by $r=$const.

III. COMPUTATIONAL METHODS

A. General

The basic strategy we adopt is to conduct random walks within the various permutational cells that lie within the various nodal regions in order to sample the *spatial* properties of these structural domains. This contrasts markedly with traditional QMC simulations where the walkers locally sample *physical* properties such as the energy or dipole moment. Each random walker in $3N$-dimensional space represents a particular configuration of electrons in an atom in three-dimensional space. An ensemble of random walkers is merely a set of different possible configurations of the electrons in a given atom. Unless otherwise stated, the walks are purely diffusive (i.e., unbiased random walks). The sampling walks are generally preceded by an equilibration walk that is designed to homogeneously distribute the walkers within a given nodal region or cell. This is accomplished by maintaining a running average of the nearest-neighbor separation between random walkers, which is stored in a circular buffer. Equilibration is signaled by the occurrence of *random* deviations from the running average over a prescribed length of the walk. Our study consists of four parts: (i) Mapping the nodal topology for Li–C; (ii) comparison of all permutational cells of a given atomic wave function (Be) to see if they are geometrically equivalent; (iii) comparison of geometric properties of a single permutational cell for a group

of first-row atoms; (iv) characterization of topological bottlenecks separating different cells having the same sign. In all four phases, we investigate the effect of using different basis sets in our trial wave functions.

We initially employed four different basis sets. The first two were taken from the literature and consisted of Clementi and Roetti's[14] double-ζ and near HF limit quadruple-ζ Slater-type orbital (STO) basis sets. The latter two were calculated using the HONDO package of computer codes[15] using a double-ζ Gaussian-type orbital (GTO) basis set (Dunning's double-ζ contraction[16] of Huzinaga's $(9s5p)$ set[17] of primitive Gaussian functions) at the restricted (RHF) and unrestricted (UHF) levels of theory. Comparison of results with these four Ψ_T's for Li showed many similarities in the geometric or topological properties. However, the average electron-nuclear distance exhibited by the double-ζ STO wave function are significantly smaller than the other three trial wave functions studied. For this reason, we employed only the STO quadruple-ζ basis set for the remainder of the study. We did not use explicit positive correlation functions (e.g., Jastrow functions) in the trial wave functions, which are commonly used in QMC, since being everywhere positive they do not affect the placement of the nodal surfaces.

B. Nodal region and cell count

We employed a cluster analysis as outlined by Ceperley[4] to count the number of nodal regions in the domain of a given wave function. All permutational cells within all nodal regions are initially populated using either of the following methods: generate all permutational copies of a series of arbitrarily chosen points or perform a guided random walk, where walkers are permitted to cross nodal boundaries. In the latter case, the walk proceeds until the walkers are distributed as $\Psi_T^2(\mathbf{R})$. After all distinct parts of configuration space have been populated, an unbiased random walk is conducted to fill homogeneously each permutational cell and region. Because nodal regions and cells may be unbound, we impose an artificial nodal boundary of $|\Psi| = 10^{-4}$. All pairs of walkers that have the same sign are then connected by a straight line (a $3N$-dimensional vector originating at walker 1 and terminating at walker 2) that is divided into equally spaced intervals (ranging from 10^{-3} to 10^{-6} bohr) at which the sign of the wave function is determined. If the sign has not changed anywhere along the line, we assign that pair of walkers to the same nodal region. This static phase of the analysis provides only an upper bound to the number of cells since it is possible for nodal crossings (an even number) to occur on a line connecting a pair of walkers that reside in the same nodal region. This can occur when the region is not simply connected as depicted by the outer region of a $2s$ hydrogenlike atomic orbital shown in Fig. 4. We define $\Omega(\mathbf{R})$ as a function which returns the label of the nodal region (or permutational cell depending upon the context) for a particular position $\mathbf{R}$ in $3N$ space. Overcounting is eliminated in two successive steps. First we employ a tree-structure clustering algorithm,[18] where if $\Omega(\mathbf{R}_1) = \Omega(\mathbf{R}_3)$ and $\Omega(\mathbf{R}_2) = \Omega(\mathbf{R}_3)$, then $\Omega(\mathbf{R}_1) = \Omega(\mathbf{R}_2)$ even when $\mathbf{R}_1$ and $\mathbf{R}_2$ were not previously equivalenced [see Fig. 4(b)]. Second, the walkers diffuse randomly within the confines of the nodal regions whereupon the clustering analysis is reinitiated for those walkers of like sign that have not yet been equivalenced [see Fig. 4(c)]. This corresponds to the use of curved paths in Ceperley's algorithm.[4] This diffuse-and-cluster routine proceeds until the number of regions returned remains constant after a prescribed number of iterations. Prior to this dynamical clustering analysis, the walkers are reequilibrated to fill each nodal volume homogeneously rather than according to $\Psi_T^2(\mathbf{R})$.

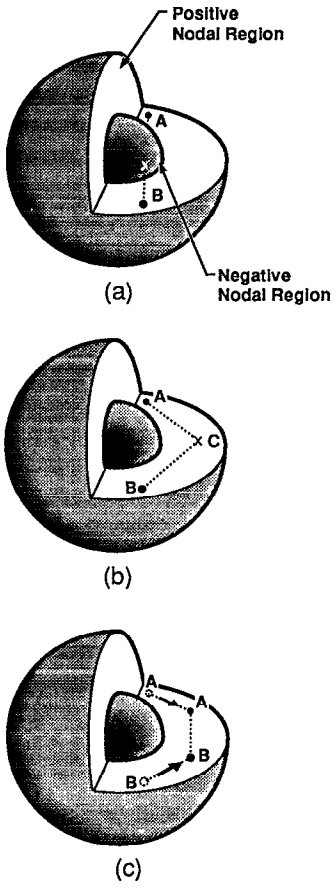

FIG. 4. Illustration of clustering algorithm in nonconvex topologies. (a) Walkers **A** and **B** are assigned to different nodal regions (not clustered); (b) walkers **A** and **B** are clustered via walker **C** into the same nodal region; (c) diffuse-and-cluster technique in which walkers **A** and **B** are clustered after diffusion to a new set of positions.

C. Topology of permutational cells

All pairs of permutational cells that have opposite sign are tested to determine if they share a common boundary. To populate each permutational cell, it is only necessary to create $N_\alpha! N_\beta!$ permutational copies of any point in $3N$ space. If this is repeated for M points, there will be M walkers populating each cell. Unfortunately, when there are more walkers than permutational cells, it may not, in general, be possible to determine whether two walkers (having the same sign) belong to the same permutational cell. This arises in part because permutational cells are not

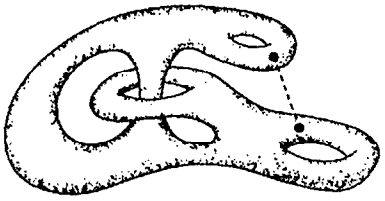

FIG. 5. Possible topology for a highly convoluted nodal region containing several permutational cells. We have depicted a line connecting two walkers in different permutational cells within a given nodal region.

delimited by nodal surfaces. Whereas, walkers may be clustered into nodal regions by the line walking algorithm (see the aforementioned), they cannot be clustered into permutational cells in this manner. This ambiguity may be removed by using only *one* set of permutational copies such that each walker defines (and is representative of) a given permutational cell.

In the high-dimensional space of the wave function domain, we must allow for the possibility of highly convoluted permutational cell topologies as illustrated in Fig. 5. For this reason, we conduct a static analysis (i.e., walkers do not diffuse) to count the number of intervening nodes between permutational cells of both like and opposite sign. First, all pairs of representative walkers are connected by a straight line. Along each line, the sign of the wave function is determined at equally spaced intervals ranging from 10^{-3} to 10^{-6} bohr. The number of nodal crossings is given by the number of times the wave function changes sign. We repeat this analysis using a different set of permutational image walkers where $|\Psi|$ is changed. If the sign of Ψ_T changes only once for any line connecting pairs of walkers between two cells (only one nodal crossing), the permutational cells are connected. This analysis is repeated, successively halving the length of the line intervals at each iteration, to ensure that intermediate nodal regions have not been overlooked (i.e., a negative region sandwiched between two positive regions). We find that the appropriate stride will vary depending upon the magnitude of $|\Psi|$ for the pair of walkers being connected. As an adjunct to this procedure, we also minimize $|\Psi|$ along the line connecting pairs of walkers. This ensures that nodal crossings are not overlooked and also provides an indication of the degree to which two permutational cells are coupled (i.e., connected by regions of high or low probability).

The determination of whether a given nodal region or permutational cell is finite (bounded volume) or infinite (unbounded volume) in extent does not actually require that the volume of a given cell is computable. Indeed it is not possible to do so strictly within a Monte Carlo framework when there are two or more positive (negative) cells. We instead exploit the relationship between average nearest neighbor separation ($\bar{\rho}$) and concentration (c) in a random fluid, which is given by[19]

$$\bar{\rho}=4\pi N D c^{-1/3N}, \tag{7}$$

where N is Avogadro's number and D is the diffusion constant. Since the number of walkers in a cell is known, we can solve for the volume of a given cell in terms of $\bar{\rho}$

$$V\alpha\bar{\rho}^{3N}. \tag{8}$$

This expression was originally derived for a bulk liquid without boundaries so we cannot insist on an exact correspondence to the present case where the nodal surfaces can exhibit arbitrary topologies. We therefore employ Eq. (8) in a qualitative fashion only as a guide to the intuitive reasoning that follows.

We assume that the *hypervolume of configuration space* enclosed by a given range of $|\Psi|\rangle$ cutoff increases exponentially with decreasing values of the cutoff for an unbounded cell or region. We start by imposing an artificial boundary to each permutational cell as defined by the minimum absolute value that the wave function can adopt. By successively halving this cutoff value, two types of behavior can be discerned: the *change* in effective volume will increase monotonically for *unbounded* cells, but will eventually taper off and go to zero for *bounded* cells. For each cutoff value, the ensemble of walkers within each cell is equilibrated prior to determining the average nearest-neighbor separations upon which volume estimates are based. Equilibrium has been attained when deviations from a running average of $\bar{\rho}$ occur randomly over a sufficiently long interval of walk time (see the aforementioned).

D. Geometric properties

During the random walk within a chosen permutational cell or entire nodal region, various geometric properties are sampled such as the average walker hyperradius, average radius for each electron, volume/surface ratio, average probability amplitudes and densities, and the center of gravity and second spatial moments of the distribution of random walkers. We shall use the phrase electron radius to refer to the electron-nuclear distance in three-dimensional physical space. The hyperradius $R_{\rm hyp}(\mathbf{R})$ of a walker located at point $\mathbf{R}$ in $3N$ space is defined in terms of the radii of the individual electrons r_i as

$$R_{\rm hyp}(\mathbf{R})=\left(\sum_{i=1}^{n\rm elec} r_i^2\right)^{1/2}. \tag{9}$$

The origin of the coordinate system in $3N$ space (termed hyperorigin) is the point (0,0,0,...,0,0,0), which physically corresponds to all N electrons located at the nucleus (for atoms) or the center of mass (for molecules). The moments do not refer to mass or charge distributions but rather to the distribution of the homogeneous nodal volume itself with respect to the various axes that define the $3N$-dimensional configuration space. Indeed, all of the aforementioned properties $\langle X\rangle$ represent spatially homogeneous averages

$$\langle X\rangle=\int_V d\mathbf{R}\, X \Big/ \int_V d\mathbf{R} \tag{10a}$$

rather than averages taken with respect to $\Psi_T^2(\mathbf{R})$, i.e.,

$$\langle X\rangle\neq\int_V d\mathbf{R}\,\Psi_T^2(\mathbf{R})X \Big/ \int_V d\mathbf{R}\,\Psi_T^2(\mathbf{R}). \tag{10b}$$

We must therefore caution against a literal interpretation of the values of the average electronic radii. It should be noted, however, that the relative values of the electronic radii are in qualitative agreement with those obtained using importance sampling. Because individual cells tend to be unbounded (see the following) artificial boundaries [as defined by a minimum value for $|\Psi(\mathbf{R})|$] must be imposed for the random walkers. Otherwise, the electronic radii, walker hyperradii, and second moments would be infinite, and the volume/surface ratio would be ill defined. Furthermore, an infinite volume is not amenable to Monte Carlo sampling unless importance sampling is used. Intuitively, the volume/surface ratio of an artificially bounded permutational cell should somehow be related to the fraction of random walkers that attempt to cross the nodal surface during a single move. This presupposes that the random walkers are homogeneously distributed within the bulk volume of the permutational cell. Since nodal surfaces serve as reflecting barriers in these simulations, the relevant quantity is the acceptance fraction of the ensemble taken as an average over the course of many moves. Quantitatively, the volume/surface ratio is given by

$$V/S=(2Dt)^{1/2}\left(\frac{N_{\rm acc}}{N_{\rm acc}+N_{\rm rej}}\right), \tag{11}$$

where the first factor is the average distance traveled during a step size of t, and the second factor is the acceptance ratio.

E. Intercell diffusion analysis

We initially populate only a single cell within either a positive or negative region. To assess the extent of diffusion between individual permutational cells of the same sign, we exploit our finding (see below) that the average radius of a given electron about the origin (i.e., the nucleus) may vary from cell to cell. As the walk proceeds, a running average is kept of the radius of each electron. At equilibrium [i.e., walkers have sampled configuration space according to $\Psi_T^2(\mathbf{R})$], all electrons should have the same average radii. We measure the extent of equilibration at a given walk time by the dimensionless quantity $\xi(t)$ which is defined as

$$\xi(t)=\frac{1}{N}\sum_{i=1}^{N}\frac{|x_i(t)-\bar{x}(t)|}{\bar{x}(t)}, \tag{12}$$

where $x_i(t)$ denotes the running average radius of electron i at time t, $\bar{x}(t)$ represents the average of the $x_i(t)$ at time t, and N is the number of electrons per walker. Because $\xi(t)$ depends only upon the relative values of the electron radii, it may be used to compare the equilibration rates that were calculated using different wave functions, walking algorithms, or type of atom. The unbiased random walk length is on the order of 3200 hartree^{-1}, where $\xi(t)$ is evaluated every 80 hartree^{-1}. Because of the much greater computational burden when gradients are computed, the importance-sampled random walk length was 400 hartree^{-1}. We repeat this procedure at a series of boundary cutoff values and propagate the walk using either an unbiased random walk or an importance-sampled random walk.

IV. RESULTS AND DISCUSSION

A. Topology

The most striking general result to emerge from the topological analysis was that although the number of allowed nodal regions ranges from a minimum of 2 to a maximum of $N_\alpha!N_\beta!$, the ground electronic states for Be–C exhibited four distinct nodal regions: two positive and two negative. Li is a special case in that it is constrained to have only two nodal regions. These two regions for Li were found to be equivalent with respect to all geometrical properties as illustrated in Table I. All four trial wave functions demonstrated agreement on this point. The four nodal regions for Be–C were found to be equivalent and this is depicted for Be in Table II. Although the number of nodal regions given by the static phase of the clustering analysis could be large, the count always converged down to four during the dynamic (diffuse-and-cluster) phase. This result is important because a single nodal surface (and hence two nodal regions) orthogonalizes the fermion ground state to the boson ground state, which is nodeless.

The presence of four nodal regions can be rationalized in a straightforward way. To study the spatial properties of the wave function, it is necessary to fix the spin coordinates of the electrons. Previously we factored the HF wave function into a product of α-spin and β-spin determinants:

$$\Psi=\det^{\alpha}(1,\ldots N_\alpha)\det^{\beta}(N_\alpha+1,\ldots N_\alpha+N_\beta). \tag{13}$$

The α and β determinants are independent since they depend upon an entirely different set of coordinates. Because Ψ must vanish when *either* determinant vanishes, there should exist one nodal hypersurface that is associated with the nodes of the α determinant for any coordinates of the β-spin electrons and another hypersurface that is associated with the nodes of the β determinant for any coordinates of the α-spin electrons. This implies that for Be and beyond, SCF wave functions should nominally exhibit at least two nodal hypersurfaces that divide configuration space into four nodal regions. These two nodal surfaces are depicted in Fig. 6. One surface corresponds to an exchange pathway for α electrons, while the second surface corresponds to an exchange pathway for β electrons. At the $3N-2$ dimensional intersection region, $\Psi(\mathbf{R})=0$ and $\nabla\Psi(\mathbf{R})=0$. Ceperley has also shown that saddle points may be found on this seam.[4] To test this notion of two independent nodal surfaces, we investigated the behavior of the α and β determinants separately for Li–C. In all cases, there were only two nodal regions found (one positive and one negative), which is consistent with the existence of a single $\alpha(\beta)$-exchange nodal hypersurface for systems of $\alpha(\beta)$ electrons only. Ceperley had found this same result for free-particle systems all of the same spin.[4]

We note that at the HF level, the full $3N-1$ nodal hypersurface for Be is known: $r_1=r_2$ and $r_3=r_4$, where 1 and 2 are α electrons and 3 and 4 are β electrons. When instantaneous Coulomb correlation between electrons is taken into account via a CI treatment, the resulting wave function can no longer be separated into α and β components. Such wave functions differ from the HF wave func-

TABLE I. Basis-set dependence of nodal properties for Li.

Property	RHF STO-DZ		RHF STO-QZ		RHF GTO-DZ		UHF GTO-DZ	
Vol/surf ratio[a]	0.075	0.075	0.080	0.080	0.080	0.080	0.080	0.080
Ψ (ave.)	$3.59E-4$	$-3.58E-4$	$3.09E-4$	$-3.09E-4$	$3.10E-4$	$-3.11E-4$	$3.11E-4$	$3.11E-4$
Ψ^2 (ave.)	$3.01E-6$	$3.10E-6$	$8.80E-7$	$8.77E-7$	$9.07E-7$	$8.95E-7$	$8.86E-7$	$9.05E-7$
Hyperradius	4.38	4.39	6.41	6.43	6.35	6.35	6.35	6.35
				Ave. elec radii[a]				
1st	0.96	3.95	1.14	6.10	1.14	6.01	1.14	6.02
2nd	3.93	0.95	6.08	1.14	6.02	1.14	6.01	1.14
3rd	1.16	1.16	1.18	1.17	1.18	1.18	1.18	1.18
				Centroid[a]				
x_1	0.00	0.00	0.00	−0.01	0.00	−0.02	0.00	−0.03
x_2	0.00	−0.01	0.00	0.01	0.00	0.01	0.00	0.00
x_3	0.00	−0.02	0.00	0.02	0.00	−0.02	0.00	0.02
x_4	0.01	0.00	−0.01	0.00	0.01	0.00	−0.02	0.00
x_5	0.01	0.00	−0.01	0.00	−0.02	0.00	0.01	0.00
x_6	0.01	0.00	0.03	0.00	−0.01	0.00	−0.03	0.00
x_7	0.00	0.00	0.00	0.00	0.00	0.00	0.00	0.00
x_8	0.00	0.00	0.00	0.00	0.00	0.00	0.00	0.00
x_9	0.00	0.00	0.00	0.00	0.00	0.00	0.00	0.00
				Second moments[b]				
x_1^2	0.37	6.35	0.52	14.35	0.52	13.88	0.52	13.90
x_2^2	0.37	6.35	0.52	14.43	0.52	13.90	0.52	13.87
x_3^2	0.37	6.32	0.52	14.35	0.52	13.83	0.52	13.93
x_4^2	6.26	0.37	14.21	0.52	13.91	0.52	13.99	0.52
x_5^2	6.32	0.37	14.32	0.52	13.87	0.52	13.91	0.52
x_6^2	6.29	0.36	14.30	0.52	13.87	0.52	13.75	0.52
x_7^2	0.57	0.57	0.56	0.56	0.56	0.56	0.56	0.56
x_8^2	0.57	0.57	0.56	0.56	0.56	0.56	0.56	0.56
x_9^2	0.57	0.57	0.56	0.56	0.56	0.56	0.56	0.56

[a]In units of bohr.
[b]In units of bohr^2.

tion in Eq. (13) in that there will be a sum of products rather than a single product of determinants. The two nodal surfaces will no longer be independent, and we cannot rule out that at the CI level the intersection seam of the nodal hypersurfaces will become a finite-valued bottleneck (saddle-point) that provides a passageway between the two parts of what is now one contiguous positive (negative) nodal region. This scenario is depicted in Fig. 7.

For all atoms studied, all nodal regions were determined to be unbounded. Since all nodal regions in the ground state are geometrically identical, and at least one region must be unbounded, then all permutational cells must be unbounded for ground-state wave functions. For excited-state wave functions, where nodal regions will no longer be constrained to be identical, *bounded* nodal regions may arise. The connectivity patterns between nodal regions seem rather trivial insofar as there are only four regions in the ground state; two positive regions that are separated by two negative regions as depicted in Fig. 6. In contrast, the connectivity patterns between permutational cells are as yet undefined and provide a fertile ground for exploration.

Permutational (exchange) symmetry requires that each nodal region contain $N_\alpha!N_\beta!/N_{\text{region}}$ permutational cells, where N_{region} gives the number of nodal regions. Li and Be are special cases insofar as they are the only systems wherein a permutational cell is also a nodal region. For B and larger systems, a nodal region will generally contain more than one permutational cell. Our results indicate that not all positive permutational cells are interconnected in the same manner. For B, all positive (negative) permutational cells are related to each other by a double permutation of electronic coordinates. There are two possibilities: a single α followed by a single β permutation or a double α permutation. Since B has only two β electrons in the ground state, a double β permutation returns the starting configuration. Line minimizations conducted between pairs of walkers of like sign demonstrated that two cells related by two α-α permutations are connected by regions of high probability, whereas two cells related by α-α, β-β permutations encounter a nodal surface along their connecting lines. We interpret this to mean that those cells related by permuting only α electrons are clustered together on one side of the topological bottleneck. In general, permutational cells of like sign may be related in two archetypal ways: (i) via an even permutation of α electrons followed by an even permutation of β electrons or (ii) via an odd permutation of α electrons followed by an odd permutation of β electrons. Based upon the foregoing evidence, we conjecture that the following property holds for fermion systems in general: permutational cells related by permutation scheme (i) are clustered together in the same

TABLE II. Geometric properties of the four nodal cells in the wave function domain of Be.

Property	Nodal cell 1		Nodal cell 2		Nodal cell 3		Nodal cell 4	
Vol./surface ratio[a]	0.008	(23)	0.010	(16)	0.008	(26)	0.008	(28)
Ψ (ave.)	$0.32E-2$	(12)	$-0.35E-2$	(9)	$-0.31E-2$	(1)	$0.30E-2$	(2)
Ω^2 (ave.)	$0.17E-4$	(9)	$0.18E-4$	(7)	$0.16E-4$	(1)	$0.15E-4$	(1)
Hyperradius[a]	4.02	(5)	3.97	(7)	3.83	(5)	3.94	(2)
			Ave. electron radii[a]					
1st	0.36	(1)	2.62	(3)	0.40	(1)	2.48	(6)
2nd	2.78	(6)	0.38	(0)	2.51	(7)	0.40	(1)
3rd	0.42	(2)	0.38	(0)	2.60	(2)	2.78	(6)
4th	2.60	(5)	2.72	(8)	0.45	(2)	0.43	(2)
			Zeroth moments[a]					
x_1	0.00	(1)	−0.05	(6)	0.02	(1)	0.12	(9)
x_2	0.00	(1)	−0.15	(9)	0.06	(2)	0.15	(10)
x_3	0.01	(1)	0.09	(8)	−0.03	(2)	−0.27	(8)
x_4	−0.04	(9)	0.00	(0)	−0.18	(12)	−0.05	(2)
x_5	0.17	(17)	0.00	(0)	0.11	(5)	0.02	(1)
x_6	−0.47	(12)	−0.02	(1)	−0.12	(6)	−0.01	(2)
x_7	0.00	(1)	0.01	(1)	−0.34	(14)	0.30	(15)
x_8	−0.07	(3)	0.01	(1)	0.17	(7)	−0.12	(17)
x_9	−0.03	(1)	0.01	(0)	0.01	(5)	0.18	(9)
x_{10}	−0.26	(10)	−0.02	(4)	−0.07	(2)	−0.02	(1)
x_{11}	0.04	(9)	0.21	(11)	−0.02	(1)	−0.09	(3)
x_{12}	−0.02	(8)	0.31	(13)	0.09	(3)	0.03	(2)
			Second moments[b]					
x_1^2	0.05	(0)	2.38	(5)	0.06	(0)	2.30	(11)
x_2^2	0.05	(0)	2.84	(14)	0.07	(1)	2.46	(19)
x_3^2	0.06	(0)	2.55	(5)	0.06	(0)	2.32	(14)
x_4^2	2.48	(16)	0.06	(0)	2.98	(35)	0.07	(0)
x_5^2	3.06	(29)	0.06	(0)	2.24	(13)	0.06	(0)
x_6^2	3.36	(31)	0.06	(0)	2.19	(12)	0.07	(1)
x_7^2	0.05	(0)	0.06	(0)	3.01	(21)	3.05	(26)
x_8^2	0.10	(3)	0.06	(0)	2.31	(9)	3.30	(40)
x_9^2	0.06	(0)	0.06	(0)	2.26	(16)	2.29	(12)
x_{10}^2	2.72	(12)	2.34	(9)	0.08	(1)	0.05	(0)
x_{11}^2	2.53	(20)	3.05	(23)	0.06	(0)	0.10	(2)
x_{12}^2	2.47	(7)	3.19	(38)	0.11	(2)	0.07	(1)

[a]In units of bohr.
[b]In units of bohr.^{2}

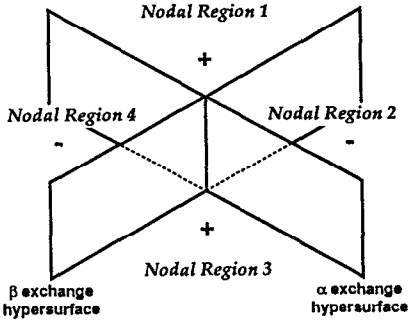

FIG. 6. Intersection of α and β nodal hypersurfaces dividing configuration space into four nodal regions.

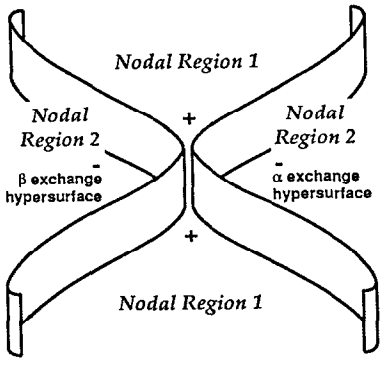

FIG. 7. Avoided crossing of nodal hypersurfaces expected for correlated wave functions. Note that there is only one nodal region of each sign. In this illustration, we have depicted only the continuity within the positive nodal region.

TABLE III. Number of node crossings between permutational cells in the wave function domain of B as a function of $|\Psi|$. One walker per nodal cell; walkers are all permutational images of each other.

Cell pair	10^{-1}	10^{-2}	10^{-4}	$\|\Psi\|^a$ 10^{-9}	10^{-11}	10^{-13}
1-2	1	1	1	1	1	1
1-3	1	1	3	1	3	1
1-4	0	2	2	0	4	2
1-5	1	1	1	1	1	3
1-6	0	0	0	0	0	4
1-7	0	2	2	2	2	2
1-8	1	3	3	3	3	3
1-9	0	2	2	2	2	2
1-10	1	3	3	3	3	3
1-11	1	1	1	3	1	1
1-12	0	2	0	2	0	2

[a]Value of $|\Psi|$ for all twelve walkers.

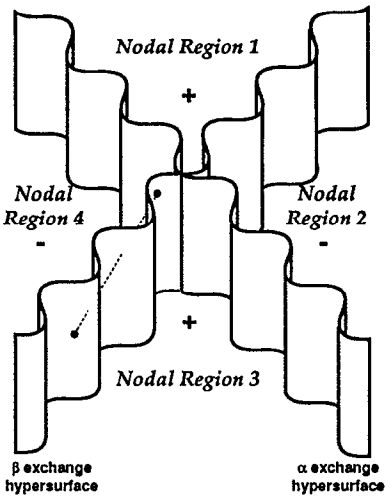

FIG. 8. Curvature of nodal hypersurfaces inferred from the number of nodal crossings between permutational cells.

nodal region, while those related by permutation scheme (ii) reside in different nodal regions. This conjecture will be tested in the intercell diffusion analysis (see the following).

Each permutational cell may be represented by a single walker. Each walker is a permutational reflection of all other walkers. The connections between the twelve permutational cells in B are shown in Table III in terms of the number of nodal crossings between their representative walkers. For the sake of clarity, we have only included a description of how a given permutational cell is connected to all others. These results nominally show that each positive (negative) cell is directly connected to all the other positive (negative) cells within the same nodal region (i.e., a straight line can be drawn between any two walkers that are related by an even permutation of electron labels such that no nodal surfaces are crossed), and that each positive (negative) cell lies adjacent to all other negative (positive) cells (i.e., a straight line can be drawn between any two walkers that are related by an odd permutation of electron labels such that there is exactly one nodal surface crossing). However, when walkers and their sets of related permutational images are allowed to migrate to regions of low probability, the interconnections between image points reveal a more complicated topology. In particular, the number of nodal crossings between a given pair of walker images tends to increase as $|\Psi|$ decreases. For B, the maximum number of crossings is three for positive–negative connections and four for positive–positive or negative–negative connections. Such behavior is consistent with the notion that nodal hypersurfaces convolute to create nonconvex nodal regions as depicted in Fig. 8. This behavior is logical from the standpoint that the nodal convolutions only affect walkers close to the nodes themselves.

B. Equivalency of permutational cells

The tiling theorem, which holds rigorously for exact wave functions,[4] states that all $N_\alpha!N_\beta!$ cells should be identical (except perhaps for a sign change). We studied the geometrical properties of the four permutational cells of Ψ_T(Be) to ascertain whether the tiling property can be extended to bound state HF wave functions. The results displayed in Table II indicate that all four cells are indeed equivalent in virtually all respects (within the statistical uncertainties of the simulation). The lone discrepancy was that the average radius of the individual electrons (i.e., electron-nuclear distance) was found to differ from cell to cell. In cell 1, the average radii are 0.4, 2.8, 0.4, 2.6 bohr for the α_1, α_2, β_1, and β_2 electrons, respectively. In cell 2, the radii of electrons 1 and 2 have been permuted; in cell 3 the radii of electrons 3 and 4 have been permuted; in cell 4 the radii of both sets of electrons have been permuted. In a crude sense, this accords with the intuitive notion that permutational cells differ only by an even or odd permutation of the electron labels (see Fig. 9). The determinantal expansion of the SCF wave function for Be is given as

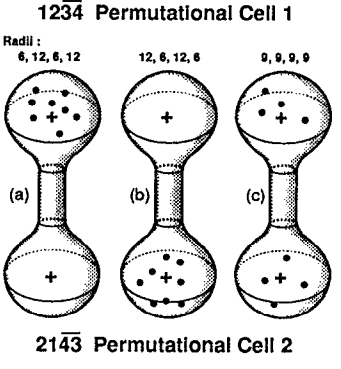

FIG. 9. The use of average electron radii about the nucleus to gauge the extent of intercell diffusion between the two positive permutational cells in the same nodal region in the wave-function domain of Be. Black dots denote random walkers in twelve-dimensional configuration space. Superscripts denote β electrons. (a) Walkers sampling permutational cell 1 yielding apparent orbital occupancy of $1s(1)2s(2)\overline{1s(3)2s(4)}$. (b) Walkers sampling permutational cell 2 yielding an apparent orbital occupancy of $1s(2)2s(1)\overline{1s(4)2s(3)}$. (c) Walkers having sampled both permutational cells equally yielding an indefinite orbital occupation.

TABLE IV. Nodal cell permutations for the wave function of B.

Orbitals[a]	Ref. conf.	Positive nodal cells Double permutations				
$1s$	α_1	α_2	α_3	α_2	α_1	α_3
$2s$	α_2	α_3	α_1	α_1	α_3	α_2
$2p$	α_3	α_1	α_2	α_3	α_2	α_1
$\overline{1s}$	β_1	β_1	β_1	β_2	β_2	β_2
$\overline{2s}$	β_2	β_2	β_2	β_1	β_1	β_1
		Negative nodal cells Single permutations			Triple permutations	
$1s$	α_2	α_3	α_2	α_1	α_3	α_3
$2s$	α_3	α_1	α_1	α_3	α_2	α_2
$2p$	α_1	α_2	α_3	α_2	α_1	α_1
$\overline{1s}$	β_1	β_1	β_2	β_2	β_2	β_2
$\overline{2s}$	β_2	β_2	β_1	β_1	β_1	β_1

[a]Overbars denote β spin orbitals.

$$\begin{aligned}\Psi(1,2,3,4) = & 1s(1)2s(2)\overline{1s(3)2s(4)} \\ & - 1s(2)2s(1)\overline{1s(3)2s(4)} \\ & - 1s(1)2s(2)\overline{1s(4)2s(3)} \\ & + 1s(2)2s(1)\overline{1s(4)2s(3)}, \end{aligned} \tag{14}$$

where the superscripted bars denote spin orbitals occupied with electrons of β spin. The average radii of the four individual electrons within a given cell are clustered into two groups: two electrons "occupying" $1s$-type orbitals and the other two electrons "occupying" $2s$-type orbitals. One anticipates that the effect of antisymmetrization is to scramble the orbital occupations such that a given electron has an equal probability of residing in any of the occupied one-particle states. However, the results in Table II provide a clear indication that within a given permutational cell, a single term in the determinantal expansion seems to predominate. For example, the two positive cells correspond to regions of $3N$ space where either the first or fourth term dominates the expansion in Eq. (14). In contrast, the nodal hypersurfaces of this antisymmetric function correspond to regions of $3N$ space where the four terms collectively balance and no single term predominates. In the case of the $3N-3$ nodal hypersurface, which corresponds to electron coincidence, all four terms are identical.

The indistinguishability of electrons must therefore be interpreted as a *global* property of the entire configuration space. We note that this property also holds for the positive half of configuration space (i.e., when both positive nodal regions are considered collectively) as well as the negative half. We illustrate this for *B* in Table IV where the twelve possible orbital occupation schemes for the five electrons are displayed. Every $\alpha(\beta)$ electron is seen to have an equal probability of appearing in each of the $\alpha(\beta)$ spinorbitals in either the positive half or negative half of configuration space separately. A similar geometrical analysis performed for Be lends credence to this idea. The results shown in Table V convincingly demonstrate that the orbital occupancies within each half of configuration space are completely scrambled so as to render the electrons indistinguishable.

TABLE V. Geometric properties of the pooled positive regions and pooled negative regions in the wave-function domain of Be. (Run parameters, 8×10^5 sample points; time step=0.05 hartree^{-1}.)

Property	Averages Positive regions		Negative regions	
Vol./surface ratio[a]	0.050	(0)[c]	0.050	(0)
Ψ (ave.)	5.21E−4	(0)	5.21E−4	(0)
Ψ^2 (ave.)	7.87E−7	(4)	7.87E−6	(4)
Hyperradius[a]	4.94	(0)	4.94	(0)
	Ave. electron radii[a]			
1st	1.85	(11)	1.97	(11)
2nd	1.99	(11)	1.86	(11)
3rd	1.84	(11)	1.87	(11)
4th	1.99	(11)	1.97	(11)
	Zeroth moments[a]			
x_1	0.00	(1)	0.01	(1)
x_2	0.00	(1)	0.01	(1)
x_3	0.00	(1)	0.01	(1)
x_4	0.00	(1)	0.00	(1)
x_5	0.00	(1)	0.00	(1)
x_6	0.00	(1)	0.01	(1)
x_7	0.00	(1)	−0.01	(1)
x_8	0.01	(1)	−0.01	(1)
x_9	0.00	(1)	0.00	(1)
x_{10}	0.00	(1)	0.00	(1)
x_{11}	0.00	(1)	0.00	(1)
x_{12}	0.01	(1)	0.00	(1)
	Second moments[b]			
x_1^2	2.08	(16)	2.22	(17)
x_2^2	2.03	(16)	2.22	(17)
x_3^2	2.03	(16)	2.22	(17)
x_4^2	2.25	(16)	2.06	(17)
x_5^2	2.24	(16)	2.06	(17)
x_6^2	2.26	(16)	2.06	(17)
x_7^2	2.04	(16)	2.08	(17)
x_8^2	2.03	(16)	2.08	(17)
x_9^2	2.05	(16)	2.07	(17)
x_{10}^2	2.25	(16)	2.23	(17)
x_{11}^2	2.25	(16)	2.25	(17)
x_{12}^2	2.25	(16)	2.21	(17)

[a]In units of bohr.
[b]In units of bohr^2.
[c]Statistical error (1 standard deviation) listed in parentheses after each quantity.

C. Permutational cell geometry for first-row atoms

The geometrical properties of a *single* permutational cell for each of the atoms Li–C are displayed in Table VI. Because nodal regions for these atomic wave functions are all unbounded (see preceding text), we have artificially delimited each region by a surface defined by $|\Psi| = 5.0 \times 10^{-2}$ rather than by the actual nodal surfaces. The centers of gravity of the permutational cells for Li–C appear to be located at the hyperorigin. Intuitively, we may expect such a result because within each permutational cell the electrons appear to have a definite orbital assignment, and each orbital is centered about the origin in 3D space. How-

TABLE VI. Geometric properties of a single nodal cell in the wave function domains of Li–C (minimum value of $|\Psi| = 5 \times 10^{-2}$).

Property	Atom			
	Li	Be	B	C
Vol./surface ratio[a]	5.9 *E*−3	1.5 *E*−3	4.0 *E*−4	6.0 *E*−4
Ψ (ave.)	1.2 *E*−1	1.1 *E*−1	6.7 *E*−2	7.2 *E*−2
Ψ^2 (ave.)	1.5 *E*−2	1.2 *E*−2	5.1 *E*−3	6.2 *E*−3
Hyperradius[a]	2.52	2.04	2.31	2.29
		Ave. electron radii[a]		
1st	2.50	1.42	1.27	0.58
2nd	0.19	0.07	1.22	1.01
3rd	0.19	1.42	0.15	0.94
4th		0.07	0.16	0.85
5th			1.32	0.15
6th				1.12
		Center of gravity[a]		
x_1-x_3	0.01, 0.00, −0.02	0.03, 0.00, 0.05	0.94, 0.03, 0.07	−0.04, −0.03, −0.04
x_4-x_6	0.00, 0.00, 0.00	0.00, 0.00, 0.00	−0.94, 0.03, 0.03	−0.36, 0.04, 0.07
x_7-x_9	0.00, 0.00, 0.00	−0.02, 0.00, 0.00	0.00, −0.01, −0.01	0.10, −0.25, 0.02
$x_{10}-x_{12}$		0.00, 0.00, 0.00	0.00, −0.02, 0.00	0.17, 0.21, 0.00
$x_{13}-x_{15}$			−0.35, 0.16, −0.03	0.00, 0.00, 0.00
$x_{16}-x_{18}$				0.19, −0.26, 0.09
		Second moments[b]		
x_1-x_3	2.25, 2.25, 2.26	0.70, 0.71, 0.72	1.10, 0.35, 0.32	0.24, 0.34, 0.09
x_4-x_6	0.01, 0.01, 0.01	0.00, 0.00, 0.00	1.13, 0.29, 0.29	0.60, 0.42, 0.25
x_7-x_9	0.01, 0.01, 0.01	0.75, 0.69, 0.69	0.03, 0.01, 0.01	0.45, 0.42, 0.25
$x_{10}-x_{12}$		0.00, 0.00, 0.00	0.01, 0.01, 0.01	0.41, 0.35, 0.22
$x_{13}-x_{15}$			0.65, 0.57, 0.68	0.01, 0.01, 0.01
$x_{16}-x_{18}$				0.44, 0.51, 0.41

[a]In units of bohr.
[b]In units of bohr^2.

ever, it does not necessarily follow that the *N*-body wave function in $3N$ space must possess the same symmetry properties as the constituent one-body, three-dimensional wave functions since the former is an antisymmetrized product of the latter. In general, the statistical error for the various quantities seems to grow larger as the size of the atom increases. The greatest relative uncertainty appears to be associated with the center of gravity of the spatial distribution, which arises from the fact that it is the only quantity that is determined by averaging both positive and negative contributions. These errors are larger for those degrees of freedom associated with electrons that occupy $2s$ or $2p$ vs $1s$ orbitals.

The volume/surface ratio monotonically decreases from Li–C. The centroid of the arbitrarily chosen permutational cells for Li and Be appears to be at the hyperorigin. The average electronic radii within a given permutational cell unambiguously indicate a well-defined orbital occupancy for Li–B. In the permutational cell for B, electrons 3 and 4 reside in core $1s$ orbitals, whereas electrons labeled 1, 2, and 5 reside in valence $2s$ or $2p$ orbitals. We may infer this behavior insofar as the average electronic radii within a chosen permutational cell cluster into two clearly distinguishable groups of vastly different radii. Yet within each group the radii are virtually identical. In the case of C, however, the electronic radii do not cluster as neatly. The two nominal core electrons (1 and 5) have vastly different radii (0.58 vs 0.15 bohr). The four valence electrons likewise exhibit a wide variation in their respective radii (0.85–1.12 bohr). We infer that the set of walkers that originally populated a *single* permutational cell in the domain of the wave function for C did not all remain with the confines of that original permutational cell (see the following).

The second principal moments of the spatial distribution indicate a nonspherical shape for the permutational cells of all four atomic wave functions. The shape appears to be ellipsoidal with the long and short axes corresponding to the degrees of freedom associated with the valence and core electrons, respectively. For a given atomic wave function, all $N_\alpha! N_\beta!$ permutational cells have the same basic shape and center of gravity and differ only by a series of rotations.

Perhaps the greatest source of error in the sampling of geometric properties of individual permutational cells is associated with random walkers hopping from one positive (negative) cell $\Omega(\mathbf{R}_1)$ into a different positive (negative) cell $\Omega(\mathbf{R}_2)$ during a given time step. This pathological behavior leads to errors in the calculated moments of the distribution and the average radii of the individual electrons. Although this behavior cannot be detected immediately after it has occurred, it may be inferred indirectly over a period of many time steps subsequent to the actual event. One measurable difference between a walker from $\Omega(\mathbf{R}_1)$ that has strayed into $\Omega(\mathbf{R}_2)$ from those that have remained confined in $\Omega(\mathbf{R}_1)$ is in their average nearest-

neighbor distances to the other walkers in $\Omega(\mathbf{R}_1)$. For this reason, every 10 steps of the walk we sampled the deviation of each walker from a running average of the average nearest-neighbor separation. At the end of the walk, those walkers with a cumulative number of *positive* deviations greater than 3 standard deviations from the average (50%) were rejected and they did not contribute to the pooled estimate of the geometrical properties.

Li and Be did not exhibit this hopping problem, whereas B and C very often did. We interpret this behavior as a measure of the density of permutational cells per nodal region in larger systems. This arises because the number of permutational cells increases factorially with the number of electrons, whereas the number of nodal regions remains constant. Li and Be possess only one permutational cell per nodal region and the two designations are synonymous in these cases. In contrast, B and C possess 3 and 12 permutational cells per region, respectively. Thus it appears that the effective *density* of permutational cells increases with the number of electrons causing larger atoms to exhibit an increased propensity for spurious hopping during the random walks. This hopping was diminished by both reducing the time step (allowing only smaller hops) and increasing the boundary cutoff value (increases the gap between adjacent cells of the same sign) such that the transition probability was noticeably decreased. However, the use of small time steps leads to inefficient sampling that required much longer time for a walk to be performed. Furthermore, the use of restrictive boundaries allows only a small region of configuration space within a given cell to be sampled. Thus we were forced to use values that represented a compromise between minimizing spurious hopping and minimizing inefficient sampling.

D. Intercell diffusion analysis

We have determined that each nodal region is comprised of one or more contiguous permutational cells and further determined how they are connected; the two nodal hypersurfaces in the ground state appear to be corrugated in the sense that they pinch off to form geometrically distinct sectors of configuration space that can be identified with the concept of permutational cells. From the standpoint of QMC simulations, it is tacitly assumed that random walkers have unrestricted mobility to explore all parts of configuration space in accordance with $\Psi_T^2(\mathbf{R})$. Indeed, this is implied by the ergodic hypothesis, which loosely states that the time average of one walker is equivalent to the ensemble average of a large collection of walkers. To test this idea, we measured the rate of intercell diffusion using either a biased or unbiased random walk, and the results are displayed in Figs. 10–14.

We logically suppose that permutational cells in close communication should be connected by regions of relatively high probability, whereas cells that are less proximate should be separated by regions of lower probability. For unbiased random walks, the presence of a dynamical bottleneck between positive (negative) cells can be inferred from the dependence of the rate of intercell diffusion on the magnitude of the boundaries for $|\Psi|$. In the case of Be

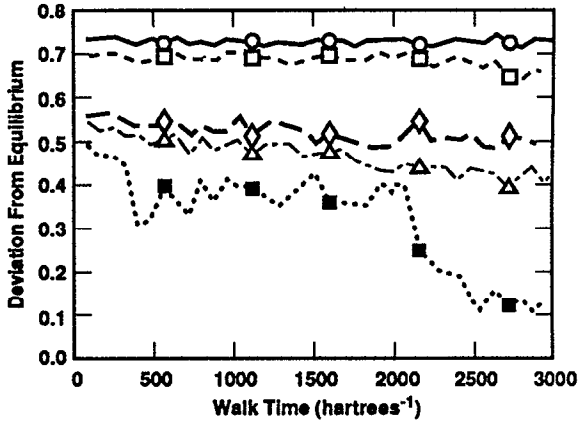

FIG. 10. Intercell diffusion analysis for Be using an unguided random walk as a function of imposed boundary cutoff. Circles, $|\Psi|_{\min}=10^{-3}$; squares, $|\Psi|_{\min}=10^{-5}$; diamonds, $|\Psi|_{\min}=10^{-7}$; triangles, $|\Psi|_{\min}=10^{-9}$; solid square, $|\Psi|_{\min}=10^{-11}$.

(Fig. 10), it is apparent that even after a long walk of 3200 hartree^{-1}, very little equilibration has occurred for cutoffs ranging from 10^{-3}–10^{-9}. It is only when the walkers are given the added freedom to wander into regions where $|\Psi|$ may be as small as 10^{-11}, does equilibration occur. Thus we may infer that a significant bottleneck is present between the two positive cells that inhibits intercell diffusion. This result is expected since for Be each permutational cell is its own nodal region, and thus the two positive cells are completely separated by intervening nodal surfaces. As shown in Fig. 6, for a positive walker to diffuse between the two positive cells, it is necessary to "hop" over a negative nodal region and thus cross two nodal surfaces. For reasonably short time steps, such hopping will only occur when walkers approach the nodal surfaces very closely.

Guided (importance-sampled) walks for Be (Fig. 11) that allow diffusion between positive and negative nodal regions appear to be 70% equilibrated on the time scale of 400 hartree.$^{-1}$ In contrast, guided walks confined to positive regions only do not appear to have diffused outside of

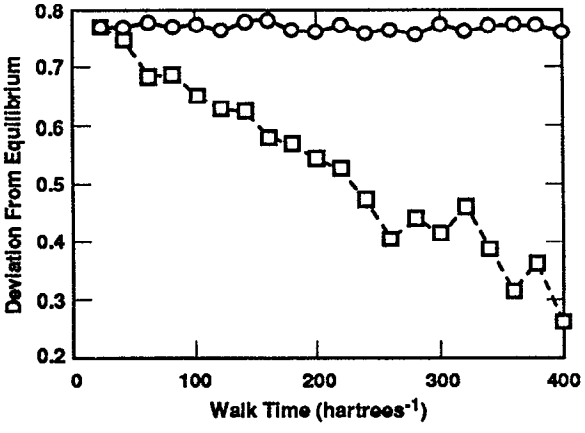

FIG. 11. Intercell diffusion analysis for Be using a guided random walk. Circles: walkers confined to the positive nodal regions. Squares: walkers permitted to cross into negative regions.

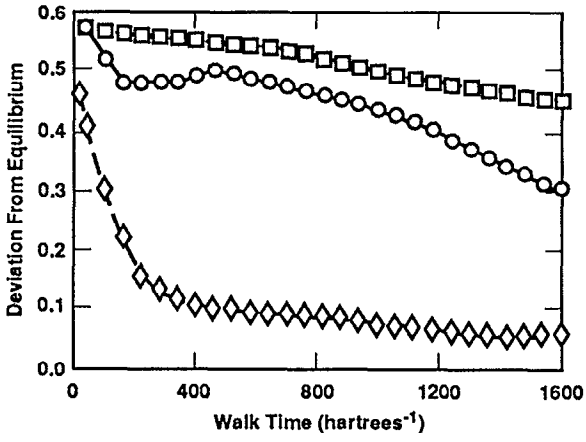

FIG. 12. Intercell diffusion analysis for the α electrons of B using an unguided random walk as a function of imposed boundary cutoff. Squares, $|\Psi|_{\min}=7.5\times10^{-2}$; circles, $|\Psi|_{\min}=5.0\times10^{-2}$; diamonds, $|\Psi|=1.0\times10^{-2}$.

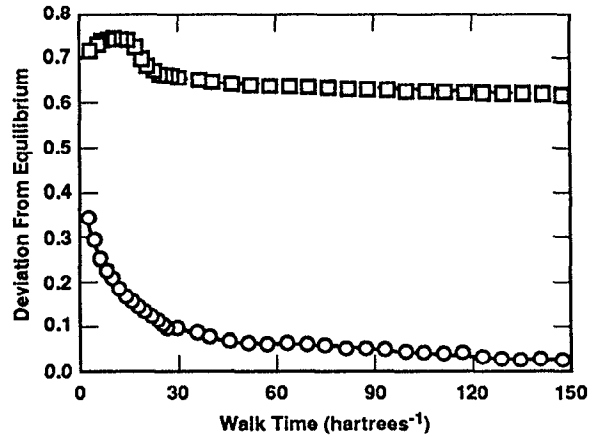

FIG. 14. Intercell diffusion analysis for C using a guided random walk with walkers confined to the positive nodal regions. Circles depict the equilibration extent of the four α electrons, and squares depict the equilibration extent of the two β electrons.

the initially populated permutational cell as evidenced by a nearly constant value of $\xi(t)$. It appears that diffusion between positive cells occurs *indirectly* through the negative regions and vice versa. Thus, *given sufficient time*, guided random walks should be capable of reliably populating configuration space in accordance with $\Psi_T^2(\mathbf{R})$ regardless of the initial distribution of walkers. In small systems, the number of walkers ($\sim$500) is greater than the number of permutational cells (e.g., Be-4, B-12, C-48) such that a random initial placement will populate virtually all cells.

For the case of B, the situation is more interesting since there are now three permutational cells in a given nodal region. When we look at the extent of equilibration of the α and β electrons separately for both the unguided (Fig. 12) and guided (Fig. 13) walks, we find that the α electrons have equilibrated (i.e., become indistinguishable in terms of orbital occupancy), whereas the β electrons have not equilibrated at all (i.e., may be distinguished

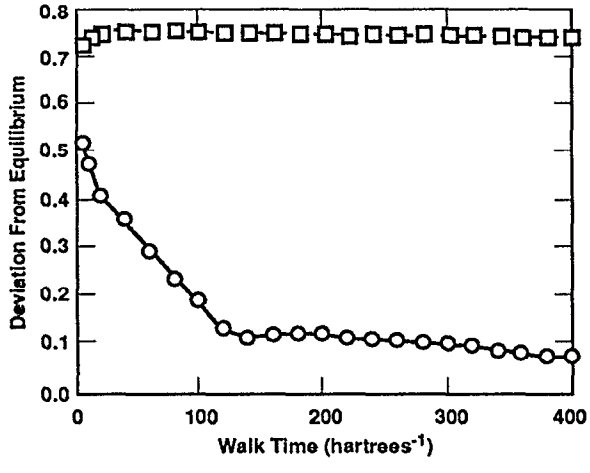

FIG. 13. Intercell diffusion analysis for B using a guided random walk with walkers confined to the positive nodal regions. Circles depict the equilibration extent of the three α electrons, and squares depict the equilibration extent of the two β electrons.

based upon orbital occupancy). This means that the permutational cells accessible to a group of walkers that began walking at the same point in configuration space differ with respect to the labeling of the α electrons but have the same β electron labeling. We anticipate this behavior for B if all permutational cells in a given region are related by a double permutation of the α electrons. Stated slightly differently, all three permutational cells in any of the four nodal regions of B have the same apparent orbital occupancy for the β electrons, hence intercell diffusion within a given nodal region does not render the β electrons indistinguishable. The same behavior was noted for C and the results of a guided walk are shown in Fig. 14.

The rather facile diffusion amongst permutational cells in a given nodal region for B undermines to some extent the distinctiveness and individuality of permutational cells. Indeed, as implied by Fig. 12, the concept of a permutational cell as a distinct contiguous sector of configuration space ceases to have meaning for those volumes of configuration space where $|\Psi|<10^{-2}$. A possible permutational cell topology to account for these results is depicted in Fig. 15. Because all well-behaved wave functions are expected to possess at least one maximum per permutational cell, these cells may be considered basins of attraction for the $N_\alpha!N_\beta!$ maxima.[20] As a walker travels away from the maximum of a given permutational cell towards the nodal surface, the apparent orbital occupancies of the electrons represented by the diffusing walker become increasingly indeterminate. In a manner of speaking, this walker increasingly becomes a citizen of all permutational cells in that nodal region. Insofar as this was the only relevant feature that distinguished one permutational cell from another, for parts of configuration space near the nodes, the concept of permutational cells is less useful.

For first-row atoms, the permutations required for a walker to travel from one permutational cell to another interchange 1*s*, 2*s*, and 2*p* orbital occupancies. Clearly, all electron permutations are not equally feasible, and the degree of feasibility is somehow related to the magnitude of

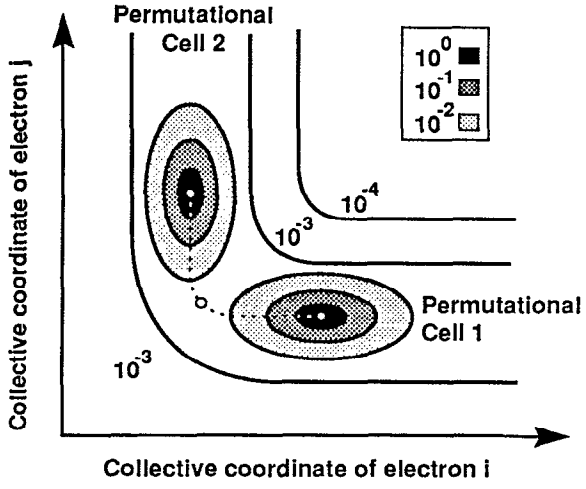

FIG. 15. Relationship between permutational cells in the same nodal region. Illustration represents a six-dimensional cross section through $3N$ configuration space.

the corresponding exchange integrals. For example, long-range van der Waals interactions entail negligible exchange between electrons formally residing on the individual monomers. In this connection, we conjecture that infeasible permutations correspond to permutational cells that are separated by some sort of bottleneck *even if these cells reside in the same nodal region*. As a corollary, the rate of intercell diffusion may be a qualitative indicator of the propensity for electron exchange. Such a bottleneck may be a manifestation of either (i) a topological constriction caused by local curvature of the nodal hypersurfaces (possibly the passageway has reduced dimensionality), or (ii) a passageway that is surrounded by regions where $\Psi_T^2(\mathbf{R})$ is uniformly small or (iii) a greater distance between the maxima of two permutational cells.

An alternative way to think about bottlenecks between permutational cells of like sign is to express the wave function in terms of its pseudopotential $U(\mathbf{R})$ defined as

$$U(\mathbf{R}) = -\ln|\Psi(\mathbf{R})|^2. \tag{15}$$

$U(\mathbf{R})$ can be considered a potential (not potential-energy) surface in the configuration space of the electrons, and is entirely analogous to the usual potential-*energy* surface in the configuration space of the nuclei. The usual notions of potential wells and barriers are applicable to the former case; maxima in $\Psi(\mathbf{R})$ correspond to minima in $U(\mathbf{R})$, and the flux bottleneck in $\Psi(\mathbf{R})$ corresponds to a saddle point in $U(\mathbf{R})$. Thus, the positive (negative) phase region consists of a series of symmetry equivalent local minima (one for each permutational cell in that region) that are separated from each other by a series of equivalent saddle points $\mathbf{R}_{sp}$. By searching $U(\mathbf{R})$ for a stationary point with one negative eigenvalue of the second derivative matrix $U''(\mathbf{R})$, it is possible to locate these bottlenecks precisely. It is tempting to extend the analogy we have drawn with nuclear potential-energy surfaces to include a transition-state theory treatment at $\mathbf{R}_{sp}$ yielding pseudoenergies and pseudoentropies of activation. The latter would require the evaluation of the translational, rotational, and vibrational partition functions corresponding to the configuration of N electrons in three-dimensional space that collectively define $\mathbf{R}_{sp}$. Because $U(\mathbf{R})$ becomes infinite at the nodes, and does not distinguish between positive and negative regions of $\Psi(\mathbf{R})$, it would not be profitable to carry out random walks in accordance with $U(\mathbf{R})$ rather than $\Psi(\mathbf{R})$.

Finally, we note that the global maximum that exists in each permutational cell may not be a single zero-dimensional point. Because atoms possess spherical symmetry, the configuration of electrons that corresponds to the maximum may be rotated with respect to the three Euler angles into a three-dimensional manifold of equivalent positions. Such rotations preserve the relative orientation among the electrons. The only symmetry operation performed upon a walker (i.e., a given configuration of electrons) capable of transporting it from one cell to another is the permutation operation. We note that a permutational exchange between electrons 1 and 2 will not preserve the relative orientation that existed previously between electrons 1 and 2 relative to electron 3. We may extrapolate these results to polyatomic systems, where the symmetry of the nuclear framework determines the lower bound to the dimensionality of the locus of global maxima within each permutational cell. The number of rotational symmetry axes of infinite order determine the dimensionality of the global maxima. Diatomic molecules possess one infinite symmetry axis, and thus the global maxima lie along a circle. In the case of H_2O, which possesses only one twofold axis of symmetry, the global maxima are defined by two zero-dimensional points. We caution that the dimensionality of the global maxima within each permutational cell must be taken as a lower bound inasmuch as there may be other symmetries independent of rotations (e.g., inversion).

V. CONCLUSIONS

Ceperley proved that all positive (negative) permutational cells are equivalent (tiling theorem) for exact wave functions.[4] Furthermore, Ceperley showed that permutational cells are interconnected for free-electron systems in which all electrons possess the same spin (i.e., one nodal hypersurface separating one positive and one negative nodal region). We have demonstrated that these properties apply to HF wave functions for Li–C. In the usual case where these atoms possess both α and β spin electrons, our results indicate that four nodal regions are formed by the intersection of two nodal hypersurfaces. We have found that nodal regions are partitioned into permutational cells that may be operationally distinguished from each other. Although all permutational cells of the same sign are geometrically equivalent, they bear different topological relationships to each other. In this connection, Ceperley's speculation[4] that bottlenecks precluding fermion exchange

may be responsible for the lack of macroscopic quantum effects in fermion systems is particularly noteworthy.

The random-walk algorithm adopted herein provides a simple and straightforward method to map the topology and geometry of the nodal regions and cells of *N*-body wave functions. This technique is readily applicable to the study of excited-state wave functions where the nodal topology is expected to be more complex (e.g., nodal regions are no longer required to be identical). Toward that end, work is currently in progress to examine the nodal properties of multideterminantal (both CI and MCSCF) wave functions of both ground- and excited-state wave functions. We anticipate that this mapping technique may provide a straightforward means to diagnose nodal pathologies in an *N*-body wave function that would render it unsuitable for use in fixed-node QMC calculations. Finally, this simulation technique is not restricted to the electronic problem and may be applied to the mapping of rovibrational wave functions as well.

ACKNOWLEDGMENTS

This research is supported in part by the Director, Office of Energy Research, Office of Basic Energy Sciences, Division of Chemical Sciences of the U.S. Department of Energy. The authors are indebted to Professor David M. Ceperley (University of Illinois) for a critical reading of this manuscript. We also thank Mr. David French (Sandia National Laboratories) for technical support in drafting the figures.

[1] J. B. Anderson, Phys. Rev. A **35**, 3550 (1987).
[2] J. B. Anderson, J. Chem. Phys. **65**, 4121 (1976).
[3] R. N. Barnett, P. J. Reynolds, and W. A. Lester, Jr., J. Chem. Phys. **82**, 2700 (1985).
[4] D. M. Ceperley, J. Stat. Phys. **63**, 1237 (1991).
[5] W. A. Lester, Jr. and B. L. Hammond, Annu. Rev. Phys. Chem. **41**, 283 (1990).
[6] J. M. Hammersley and D. C. Handscomb, *Monte Carlo Methods* (Wiley, New York, 1964).
[7] K. E. Schmidt and M. H. Kalos, in *Monte Carlo Methods in Statistical Physics II*, Vol. XIV of Topics in Current Physics, edited by K. Binder (Springer-Verlag, New York, 1984).
[8] D. M. Ceperley and B. J. Alder, J. Chem. Phys. **81**, 5833 (1984).
[9] (a) M. H. Kalos, J. Stat. Phys. **63**, 1269 (1991); (b) R. Bianchi, D. Bressanini, P. Cremaschi, and G. Morosi, Chem. Phys. Lett. **184**, 343 (1991); (c) J. B. Anderson, C. A. Traynor, and B. M. Boghosian, J. Chem. Phys. **95**, 7418 (1991).
[10] See, for example, M. Hoffmann-Ostenhof and T. Hoffmann-Ostenhof, Commun. Math. Phys. **117**, 49 (1988); H. Donnelly and C. Fefferman, J. Am. Math. Soc. **3**, 333 (1990).
[11] D. J. Klein and H. M. Pickett, J. Chem. Phys. **64**, 4811 (1976).
[12] (a) M. Caffarel and P. Claverie, J. Chem. Phys. **88**, 1088 (1988); (b) M. Caffarel, P. Claverie, C. Mijoule, J. Andzelm, and D. R. Salahub, J. Chem. Phys. **90**, 990 (1989).
[13] P. R. Bunker, *Molecular Symmetry and Spectroscopy* (Academic, New York, 1979), Chap. 6.
[14] E. Clementi and C. Roetti, *Atomic Data and Nuclear Data Tables* (Academic, New York, 1974), Vol. 14, Nos. 3–4.
[15] M. Dupuis, J. D. Watts, H. O. Villar, and G. J. B. Hurst, HONDO 7.0 (IBM Corp., Kingston, NY, 1987).
[16] T. H. Dunning, J. Chem. Phys. **53**, 2823 (1970).
[17] S. Huzinaga, J. Chem. Phys. **42**, 1293 (1965).
[18] W. H. Press, B. P. Flannery, S. A. Teukolsky, and W. T. Vetterling, *Numerical Recipes* (Cambridge University Press, Cambridge, 1989).
[19] S. Chandrasekhar, Rev. Mod. Phys. **15**, 1 (1943).
[20] D. M. Ceperley (private communication).